

# Use of digital webcam images to track spring green-up in a deciduous broadleaf forest

Andrew D. Richardson · Julian P. Jenkins ·  
Bobby H. Braswell · David Y. Hollinger ·  
Scott V. Ollinger · Marie-Louise Smith

Received: 5 October 2006 / Accepted: 30 December 2006 / Published online: 7 March 2007  
© Springer-Verlag 2007

**Abstract** Understanding relationships between canopy structure and the seasonal dynamics of photosynthetic uptake of CO<sub>2</sub> by forest canopies requires improved knowledge of canopy phenology at eddy covariance flux tower sites. We investigated whether digital webcam images could be used to monitor the trajectory of spring green-up in a deciduous northern hardwood forest. A standard, commercially available webcam was mounted at the top of the eddy covariance tower at the Bartlett AmeriFlux site. Images were collected each day around midday. Red, green, and blue color channel brightness data for a 640 × 100-pixel region-of-interest were extracted from each image. We evaluated the green-up signal extracted from webcam images against changes in the fraction of incident photosynthetically active radiation that is absorbed by the canopy ( $f_{\text{APAR}}$ ), a broadband normalized difference vegetation index (NDVI), and the light-saturated rate of canopy photosynthesis ( $A_{\text{max}}$ ), inferred from eddy flux measurements. The relative brightness of the green channel (green %) was relatively stable through the winter months. A steady rising trend in green % began around day 120 and continued through day 160, at which point a stable plateau was reached. The relative brightness of the blue channel

(blue %) also responded to spring green-up, although there was more day-to-day variation in the signal because blue % was more sensitive to changes in the quality (spectral distribution) of incident radiation. Seasonal changes in blue % were most similar to those in  $f_{\text{APAR}}$  and broadband NDVI, whereas changes in green % proceeded more slowly, and were drawn out over a longer period of time. Changes in  $A_{\text{max}}$  lagged green-up by at least a week. We conclude that webcams offer an inexpensive means by which phenological changes in the canopy state can be quantified. A network of cameras could offer a novel opportunity to implement a regional or national phenology monitoring program.

**Keywords** AmeriFlux · Bartlett Experimental Forest · Broadband normalized difference vegetation index · Digital camera · Eddy covariance · Phenology

## Introduction

Phenological records of dates of flowering and leaf-out have traditionally been kept through careful and patient field observations, sometimes as a hobby by individuals (e.g., Fitter and Fitter 2002), or by generations within the same family (e.g., the Marsham family records, which extend from 1736 to 1958; see Sparks and Menzel 2002). Although historically the domain of amateur naturalists, phenology has recently attracted widespread attention because these life cycle events have been shown to be robust indicators of the effects of climate change, especially recent warming trends (Fitter and Fitter 2002; Peñuelas et al. 2002; Badeck et al. 2004; Chuine et al. 2004).

For forest canopies, the phenological patterns of spring green-up and autumn senescence (e.g., Richardson et al.

---

Communicated by Russell Monson.

---

A. D. Richardson (✉) · J. P. Jenkins · B. H. Braswell ·  
S. V. Ollinger  
Complex Systems Research Center,  
University of New Hampshire, Morse Hall,  
39 College Road, Durham, NH 03824, USA  
e-mail: andrew.richardson@unh.edu

D. Y. Hollinger · M.-L. Smith  
USDA Forest Service,  
Northern Research Station, 271 Mast Road,  
Durham, NH 03824, USA

2006a) have added importance because growing season length represents a key constraint on primary productivity (Lieth 1975; Running and Nemani 1991; White et al. 1999; Baldocchi et al. 2001; Churkina et al. 2005). An early finding from the Harvard Forest AmeriFlux site was that growing season length, which was controlled by inter-annual variation in climate (especially springtime temperature), explained in large part the year-to-year variation in gross photosynthesis (Goulden et al. 1996). More broadly, gradual increases in growing season length at high latitudes in the northern hemisphere have resulted in increased primary productivity over the last two or three decades (Lucht et al. 2002; Nemani et al. 2003). Beyond C cycle impacts, patterns of canopy development and senescence have also been linked to seasonal changes in surface resistance and the turbulent exchange of water and energy (Moore et al. 1996; Sakai et al. 1997; Hollinger et al. 1999).

The state of the canopy thus exerts a major control on spatial and temporal patterns of the forest–atmosphere exchange of C and water. To improve understanding of both seasonal patterns, and responses to interannual and long-term variation in climate, a variety of new approaches to describe canopy state have been employed. For example, satellite remote sensing provides spatially extensive information from which signals of green-up and senescence can be extracted (White et al. 1997; Jenkins et al. 2002; Schwartz et al. 2002; Fisher et al. 2006). Limitations of satellite remote sensing of phenology include tradeoffs between spatial and temporal resolution, as well as frequent image contamination by aerosols and clouds, and effects of changes in viewing angle. In situ (tower based) optical or radiometric methods, which might be described as “near” remote sensing, can be used to characterize the phenological patterns within individual stands (Moore et al. 1996; Huemmrich et al. 1999; Wythers et al. 2003; Wang et al. 2004; Jenkins et al. 2007). Two commonly used optical indices are the fraction of incident photosynthetically active radiation that is absorbed by the canopy ( $f_{\text{APAR}}$ ), and a broadband normalized difference vegetation index (broadband NDVI) calculated from the albedos of visible and global solar radiation (Qi et al. 1995; Huemmrich et al. 1999; Wang et al. 2004; Jenkins et al. 2007). An advantage of these tower-based approaches is that these data can be obtained continuously and at a high temporal resolution (e.g., half hourly if desired), but a drawback is that they cannot be used to obtain an integrated, regional- (or larger) scale perspective, as is the case with satellite remote sensing platforms (e.g., Landsat, MODIS).

The worldwide network of eddy covariance sites at which surface–atmosphere exchange of CO<sub>2</sub>, water and energy is being continuously monitored (FLUXNET and associated regional networks, such as AmeriFlux; see

Baldocchi et al. 2001) offers a tremendous opportunity for researchers to investigate relationships between canopy phenology and whole-ecosystem physiology (e.g., Moore et al. 1996; Sakai et al. 1997; Wang et al. 2004; Hill et al. 2006; Jenkins et al. 2007) across a range of ecosystem types and bioclimatic regions.

The factors controlling the onset of C uptake in the spring are still poorly understood (Sun et al. 2003). Using flux data from a range of deciduous forests, Baldocchi et al. (2005) demonstrated that the date at which the spring transition from CO<sub>2</sub> source to sink occurred generally corresponded to the point in time at which the mean daily soil temperature equaled the main annual air temperature. However, a more mechanistic understanding of relationships between canopy structure and the seasonal dynamics of CO<sub>2</sub> uptake requires improved knowledge of canopy phenology. Thus, Baldocchi et al. (2005) encouraged FLUXNET member sites to “install video cameras... and record the state of the canopy each day”.

In response to this call, we installed a webcam on our flux tower at the Bartlett Experimental Forest (a deciduous forest located in the northeastern United States) at the end of the growing season in 2005. In the present study, we present an analysis of data extracted from webcam images recorded each day between January and July (days 1–209) 2006, covering the winter (before day 120), green-up (days 120–160), and summer (after day 160) phases of canopy state. The time series derived from the images are then compared to simultaneous measurements of  $f_{\text{APAR}}$  and broadband NDVI made at the same site with tower-mounted radiometric instruments, using a simple logistic model to determine the characteristics (timing and steepness of the green-up trajectory) of the underlying phenological signal. Finally, patterns of green-up are compared to changes in physiological activity of the canopy, inferred from eddy flux measurements of forest–atmosphere CO<sub>2</sub> exchange.

## Materials and methods

### Study site

The Bartlett Experimental Forest (44°17'N, 71°3'W) is located within the White Mountain National Forest in north-central New Hampshire, USA. The climate is humid continental with short, cool summers (mean July temperature, 19°C) and long, cold winters (mean January temperature, –9°C) (for additional site information, see <http://www.fs.fed.us/ne/durham/4155/bartlett.htm>). At low- to mid-elevation, vegetation is dominated by northern hardwoods (American beech, *Fagus grandifolia*; sugar maple, *Acer saccharum*; and yellow birch, *Betula alleghaniensis*),

with some red maple (*Acer rubrum*) and paper birch (*Betula papyrifera*) also present. Conifers (eastern hemlock, *Tsuga canadensis*; eastern white pine, *Pinus strobus*) are occasionally found intermixed with the more abundant deciduous species but are generally confined to the lowest elevations.

A 26.5-m-high tower was installed in a low-elevation northern hardwood stand in November 2003, for the purpose of making eddy covariance measurements of forest-atmosphere CO<sub>2</sub>, H<sub>2</sub>O and energy exchange. Continuous flux and meteorological measurements began in January 2004, and are ongoing (data are available at the AmeriFlux web page, <http://www.public.ornl.gov/ameriflux/>). In the vicinity of the tower, the forest is predominantly classified into red maple, sugar maple, and American beech forest types.

#### Eddy covariance measurements of CO<sub>2</sub> flux

The forest-atmosphere CO<sub>2</sub> flux (net ecosystem exchange; NEE) was measured at a height of 25 m with an eddy covariance system consisting of a model SAT-211/3K 3-axis sonic anemometer (Applied Technologies, Longmont, Colo.) and a model LI-6262 fast response CO<sub>2</sub>/H<sub>2</sub>O infrared (IR) gas analyzer (Li-Cor, Lincoln, Neb.), with data recorded at 5 Hz and fluxes (covariances) calculated every 30 min. The instrument configuration, calibration protocol, QA/QC, and data processing procedures were identical to those used at the Howland AmeriFlux site in central Maine, and have been documented in detail elsewhere (Hollinger et al. 2004).

We used a simple model to partition NEE into gross canopy photosynthesis ( $P_{\text{gross}}$ ) and ecosystem respiration ( $R_{\text{eco}}$ ) (Eq. 1a).  $P_{\text{gross}}$  is described by the commonly used, two-parameter, Michaelis-Menten light response function (Eq. 1b; e.g., Hollinger et al. 2004).

$$\text{NEE} = P_{\text{gross}} + R_{\text{eco}} \quad (1a)$$

$$P_{\text{gross}} = A_{\text{max}} \times \frac{\text{PPFD}}{K_m + \text{PPFD}} \quad (1b)$$

Here,  $A_{\text{max}}$  is the theoretical light-saturated rate of canopy photosynthesis,  $K_m$  is the half-saturation point of the light response function, and  $R_{\text{eco}}$  is treated as a constant. A separate set of model parameters was fit to each day's data, and maximum likelihood parameter estimates were obtained using weighted absolute deviations optimization (see Hollinger and Richardson 2005; Richardson et al. 2006b). Only daytime measurements [photosynthetic photon flux density (PPFD) > 5 mmol m<sup>-2</sup> s<sup>-1</sup>] were used, and if fewer than ten measurements were available, then no parameters were fit for that particular day.

#### Radiometric measurements

To complement the continuous eddy covariance measurements, a full suite of radiometric instruments was installed over the course of the first season of measurements. For a complete description of the arrangement of these instruments on the tower, and in the forest below, see Jenkins et al. (2007), as only a brief overview will be given here. Individual quantum sensors (model 190SA; Li-Cor) were used to measure incident ( $Q_{\text{incident}}$ ) and canopy-reflected ( $Q_{\text{reflected}}$ ) PPF (μmol quanta m<sup>-2</sup> s<sup>-1</sup>, 400–700 nm), while a circular array (radius = 15 m) of six quantum sensors, centered on the tower, measured below-canopy ( $Q_{\text{transmitted}}$ ) PPF. A pair of pyranometers (model CM3; Kipp and Zonen, Delft, Netherlands) measured incident ( $R_{\text{incident}}$ ) and canopy-reflected ( $R_{\text{reflected}}$ ) global radiation (W m<sup>-2</sup>, 305–2,800 nm). A sunshine sensor (model BF3; Delta-T Devices, Cambridge, UK) measured the direct beam and diffuse components of incident photosynthetically active radiation. Instruments were connected to a data logger (model CR-10; Campbell Scientific, Logan, Utah), which recorded measurements every 5 s and output half-hourly summary data (mean, maxima, and SDs) to final storage. For this analysis, we used only radiometric data collected between 1000 and 1400 h eastern time (EST).

Calculation of  $f_{\text{APAR}}$  (Eq. 2) and broadband NDVI (Eq. 3) follows Jenkins et al. (2007).

$$f_{\text{APAR}} = \frac{Q_{\text{incident}} - Q_{\text{reflected}} - Q_{\text{transmitted}}}{Q_{\text{incident}}} \quad (2)$$

and

$$\text{broadband NDVI} = \frac{\rho_{\text{NIR}} - \rho_{\text{VIS}}}{\rho_{\text{NIR}} + \rho_{\text{VIS}}} \quad (3)$$

where

$$\rho_{\text{VIS}} = \frac{Q_{\text{reflected}}}{Q_{\text{incident}}} \quad (4a)$$

and

$$\rho_{\text{NIR}} = 2 \times \left( \frac{R_{\text{reflected}}}{R_{\text{incident}}} \right) - \rho_{\text{VIS}}. \quad (4b)$$

Note that both  $f_{\text{APAR}}$  and broadband NDVI are unit-less ratios. The approach to calculating broadband NDVI differs slightly in procedure (although the results are virtually identical) from the method used by Huemmrich et al. (1999), who converted  $Q$  from micromols of photons m<sup>-2</sup> s<sup>-1</sup> to W m<sup>-2</sup> by assuming a constant energy conversion factor, and then differenced the global radiation irradiance and the converted  $Q$  irradiance to estimate the near IR

irradiance (both incoming and reflected) and thus calculate  $\rho_{\text{NIR}}$ .

### Webcam images

We used a standard, commercial webcam (model 211; Axis Communications, Lund, Sweden). The camera features a Sony Corp. 1/4" Wfine progressive scan red green blue (RGB) silicon charge coupled device. Red, green, and blue channels have peak sensitivities at wavelengths of 620, 540, and 470 nm, respectively, with relative responses >80% for bands 590–660, 520–570, and 440–480 nm (full technical specifications are available online, see Rev. E00343A0Y, available at <http://www.products.sel.sony.com/semi/PDF/ICX098BQ.pdf>). An IR cut filter (Schott BG–39, peak transmittance at 500 nm and transmittance >80% for 400–560 nm) in the camera lens is used to block IR radiation (wavelengths >700 nm).

In October 2005, we mounted the camera in a weatherproof enclosure (model 290B) immediately below the top of the tower. The camera was pointed north, and set at an angle of 20° below horizontal. The field of view was approximately 60°. Because the camera position was fixed, the field of view was more or less identical from day to day, although very minor changes occurred when the camera was periodically re-focused.

The camera was connected to a wireless local area network, and at the Bartlett Experimental Forest HQ station, a personal computer running camera image-capture software (Active WebCam; PY Software, Etobicoke, Canada) recorded a series of images at approximately 15-min intervals between ~1230 and ~1345 h EST each day. Digital images were archived as minimally compressed JPEGs (640 × 480-pixel resolution, with three channels of 8-bit RGB color information) for subsequent processing. Filenames included a date and time stamp for easy reference.

The present study was based on analysis of 868 such images, recorded between day 1 and day 209 in 2006. On average, there were four pictures per day, but unavoidable network connectivity problems resulted in occasional gaps in the webcam data record. No images were available on 31 days (~15%) of the data record. The longest gap without a picture was 4 days (day 96–99).

The camera features a variable aperture lens that responded to ambient light levels; thus, the brightness of any individual pixel is not a direct measure of surface radiance per se. Furthermore, image quality was sometimes adversely affected by variable light conditions, rain, snow, low clouds, fog, or condensation on the window of the camera housing. However, there was no selective editing or artificial enhancement of any of the archived images before the image analysis was conducted, and no smoothing or

filtering of the time series resulting from the image analysis. We believe that maintaining this level of objectivity is important because it ensures that results of comparable quality should be readily obtainable at other sites or by other researchers.

### Image analysis

A custom script was written to process the digital image files in MATLAB (R2006a; The MathWorks, Natick, Mass.). The digital camera images were sequentially read, and the date and time at which the picture was taken parsed from the filename. Analysis was conducted on a rectangular region-of-interest (ROI) that spanned the full width of the picture (640 pixels) and extended vertically from pixel 250 to 350 (see Fig. 1a). The area was selected as a compromise between maximizing the amount of deciduous forest canopy included for analysis, while at the same time avoiding mountains and sky above the ROI and understory or forest floor (covered by snow in winter) below the ROI. Camera color channel information (digital numbers; DNs) was extracted from the JPEG file and averaged across the ROI (and then across multiple images on a given day) for each of the three separate color channels (red DN, green DN and blue DN). The overall brightness (i.e., total RGB DN) of the ROI was calculated as in Eq. 5, and was then used to calculate the relative (or normalized) brightness of each channel (i.e., channel %) as in Eq. 6:

$$\text{Total RGB DN} = \text{Red DN} + \text{Green DN} + \text{Blue DN} \quad (5)$$

$$\text{Channel \%} = \frac{\text{Channel DN}}{\text{Total RGB DN}} \quad (6)$$

### Identification of indicators of spring green-up phenology

To characterize the patterns of green-up phenology, as reflected by springtime changes in webcam and radiometric indices, as well as  $A_{\text{max}}$ , we fit a simple sigmoid-shaped logistic function (Eq. 7) to each time series. The logistic model has been used previously to characterize canopy development (Richardson et al. 2006a), and is commonly used in growth modeling applications (Sit and Poulin-Costello 1994).

$$f(x) = a + \frac{b}{1 + e^{(c-dx)}} \quad (7)$$

The  $a$  and  $b$  parameters control the lower ( $a$ ) and upper ( $a + b$ ) limits of the function, whereas changes in

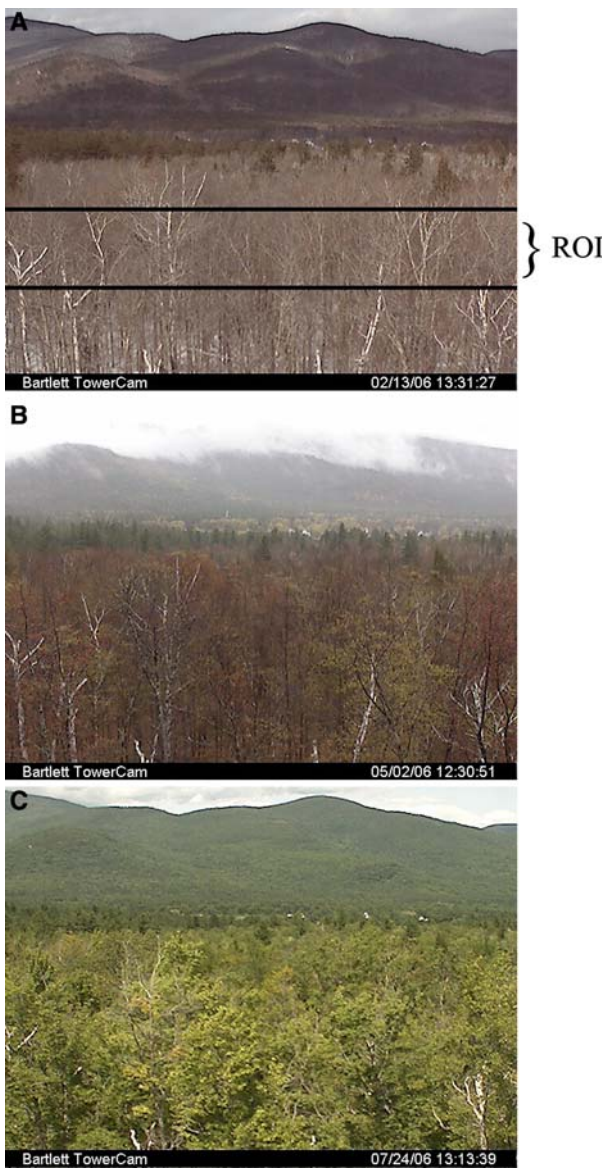


**Fig. 1** Sample webcam images showing **a** winter (day 44), **b** early spring (day 123), and **c** summer (day 206) canopy states. Pictures were taken looking north from the top (26 m) of the Bartlett AmeriFlux tower. The mask denoting the region-of-interest (ROI) selected for image analysis is indicated in **a**

the *c* parameter cause parallel shifts in the response to the driving variable *x*, and changes in the *d* parameter affect the overall steepness of the response to the driving variable. The day of year ( $\psi$ ) at which  $f(x)$  achieves its half-maximum, i.e., when  $f(x) = a + (b/2)$ , is given by  $\psi = c/d$  (see Richardson et al. 2006a). Because there were secondary patterns not associated with changes in canopy state that appear in the wintertime data for the  $f_{APAR}$  and broadband NDVI time series, only data from day 100 onwards were used for model parameterization.

## Results

### Qualitative patterns

The foreground of webcam images from the top of the Bartlett flux tower during the winter and early spring (Fig. 1a) is dominated by the gray, leafless branches of the deciduous northern hardwood forest canopy, and patches of snow are seen on the ground below. In the distance, a prominent row of tall white pine is visible in front of the forested hills rising up on the other side of the valley.

The onset of spring is marked by a change in coloration: reds and yellowish greens replace the grays of winter, as flowers (those of the red maple contributing to the reddish tinge) and leaves begin to emerge; these are clearly visible by day 123 (Fig. 1b). Development of the canopy is somewhat patchy, as species differ in the timing and rate of leaf expansion. The fully developed canopy appears as a mottled mixture of various shades of green (e.g., day 205, Fig. 1c).

### Raw (DN) and normalized (%) color channel time series

While the above patterns can be easily detected by the human eye, they were not especially obvious or well-defined in the DN time series of the red, green, and blue channels across the masked region-of-interest (Fig. 2). Whereas both red and blue DN values appeared to decrease slightly after day 120 (Fig. 2a, c), there was no clear seasonal pattern in green DN, which was relatively stable over the 7-month period of study (Fig. 2b). In other words, it appeared that the dominant springtime signal as represented by the camera record was not so much that the canopy became more green (in terms of absolute brightness), but rather that it became less red and less blue (and hence relatively more green). Based on this observation, we computed a difference index (2G\_RBi) as the difference of the divergence of both red from green and blue from green, using absolute channel brightnesses as in Eq. 8:

$$\begin{aligned}
 2G\_Ri &= (\text{green DN} - \text{red DN}) + (\text{green DN} - \text{blue DN}) \\
 &= 2 \times (\text{green DN}) - (\text{red DN} + \text{blue DN})
 \end{aligned}
 \tag{8}$$

Compared to any of the individual channel brightness values (Fig. 2a–c), 2G\_RBi quite clearly resolved changes in canopy state related to emergence from winter dormancy and spring onset of canopy development (Fig. 2d). The index was relatively stable during the winter, and then increased sharply beginning around day 120. A stable summertime plateau was reached around day 160.

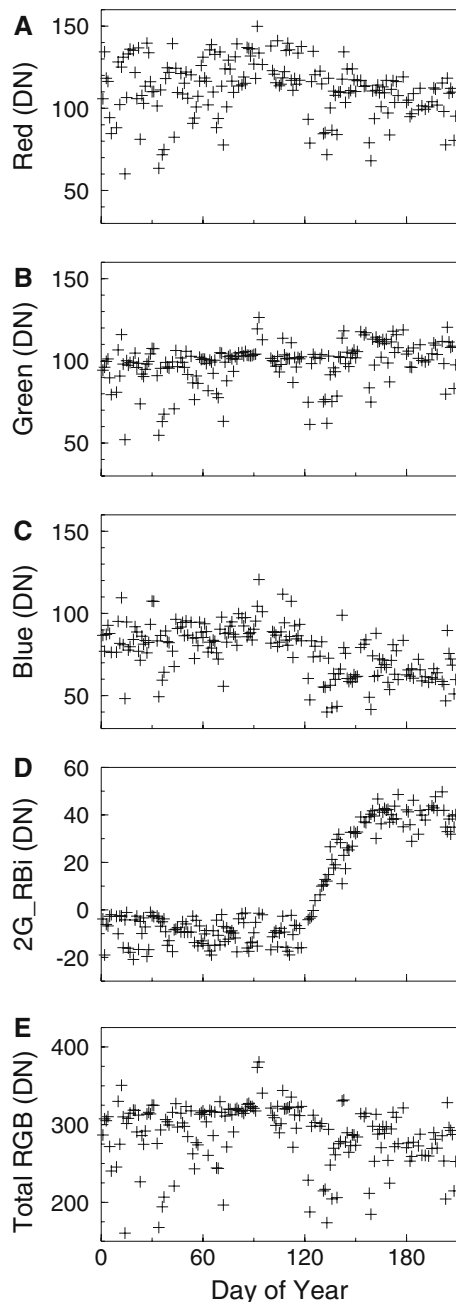


**Fig. 2a–e** Time series of channel brightness values (digital numbers; DN) for a masked  $640 \times 100$ -pixel region-of-interest in the foreground of images from the Bartlett AmeriFlux tower webcam. **a** Red DN, **b** green DN, **c** blue DN, **d** the index calculated from channel brightness values ( $2G\_Rb_i = 2 \times (\text{green DN}) - (\text{red DN} + \text{blue DN})$ ), **e** total red green blue (RGB) DN = red DN + blue DN + green DN. Note that with the exception of the total divergence of red from green and blue from green ( $2G\_Rb_i$ ), pronounced day-to-day variation in overall brightness largely masks seasonal patterns associated with spring green-up, which occurs between days 120 and 160

Extraction of a phenology signal from these data was complicated by the large day-to-day variability of each channel, and the overall brightness of the image, i.e., total

RGB DN, which varied by more than twofold (Fig. 2e). This variability can be attributed to a number of factors, including both the quantity and quality of incident solar radiation, and the internal camera response (e.g., variable lens aperture). For example, during the winter (before day 120) and green-up (day 120–160) phases there was a linear relationship ( $r > 0.60$  during each phase) between the incident PPFD and total RGB DN for PPFD  $< 1,000 \mu\text{mol m}^{-2} \text{s}^{-1}$ . In other words, below a threshold value of about one-half full sun, overall image brightness increased with the quantity of incident solar radiation.

The normalized color channel brightnesses (i.e., red %, green %, and blue %) eliminate the variability associated with overall brightness, and thus more clearly reveal seasonal patterns (compare Fig. 3 with Fig. 2). Apart from an abrupt decline at about day 150, seasonal variation in red % (Fig. 3a) was less pronounced compared to the other two normalized channels. On the other hand, green %, which was quite stable during the winter phase, began a steady rising trend around day 120, which lasted until a stable plateau was reached at about day 160 (Fig. 3b). The pattern for blue % (Fig. 3c) was similar to that for green %, but in the opposite direction. There was also much more day-to-

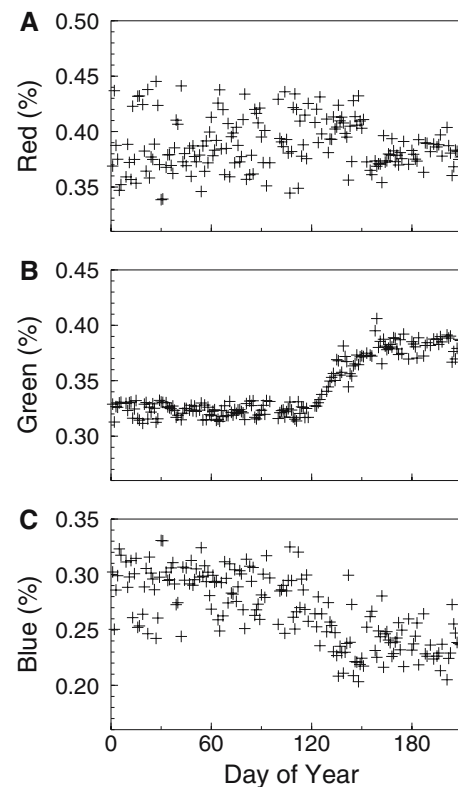


**Fig. 3a–c** Time series of normalized webcam channel brightness values (i.e., channel % = channel DN/total RGB DN) for a masked  $640 \times 100$ -pixel region-of-interest in the foreground of images from the Bartlett AmeriFlux tower webcam. **a** Red %, **b** green %, **c** blue %. For abbreviations, see Fig. 2

day variability in the blue % signal. Residual variation (around the overall trajectory) in these time series of normalized brightnesses can be partially attributed to day-to-day variation in the quality, or spectral distribution, of incident solar radiation, since this will affect the color balance of the webcam images. Changes in the direct beam:total PPFD ratio affect the spectral distribution of incident radiation (Gates 1966), and changes in the spectral distribution should be manifest as changes in the PPFD:global radiation ratio. During the winter months, red % was positively correlated ( $r = 0.81$ ), and both green % ( $r = -0.79$ ) and blue % ( $r = -0.80$ ) were negatively correlated, with the direct beam:total PPFD ratio (Fig. 4a). During the same time period, red % was negatively correlated ( $r = -0.55$ ), whereas green % and blue % were both positively correlated ( $r = 0.65$  and  $0.51$ , respectively), with the PPFD:global radiation ratio (Fig. 4b). The above observation that the time series of blue % was more variable than that of green % can thus be partially attributed to the fact that blue % was more sensitive (compared to green %) to changes in the quality of incident radiation.

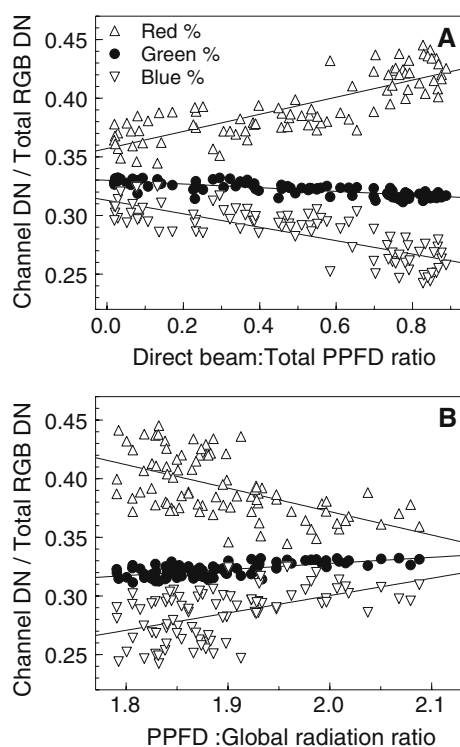


**Fig. 4a, b** Relationships between the spectral distribution, or quality, of incident solar radiation and normalized webcam channel brightness values (i.e., channel % = channel DN/total RGB DN). Data are shown for the winter (before day 120) phase, prior to spring green-up, at the Bartlett AmeriFlux tower. Indirect measures of the quality of solar radiation are: **a** ratio of direct beam to total photosynthetic photon flux density (PPFD), and **b** ratio of PPFD to global radiation. For other abbreviations, see Fig. 2

### Identifying the green-up signal

The green-up patterns indicated by 2G\_RBi and green % were almost identical; sigmoid phenology model (Eq. 7) parameters  $c$  and  $d$  were extremely similar, and the half-maximum date ( $\psi$ ) was the same (day 133) (Table 1). The overall fit of the model was somewhat better for 2G\_RBi than green % ( $R^2 = 0.945$  vs. 0.909).

On the other hand, the signal-to-noise ratio for blue % was considerably lower than for green % (i.e., the seasonal signal was smaller, and the day-to-day residual variation larger); as a result, the sigmoid phenology model was unable to account for a large proportion of the variance in blue % ( $R^2 = 0.47$ ). The changes in blue % during the green-up phase occurred sooner [the half-maximum ( $\psi$ ) was reached 8 days earlier] and more rapidly (the parameter  $d$ , which controls the overall slope, was more than twice as large) than the corresponding changes in green % (Table 1). In fact, increases in blue % were virtually complete (having reached ~90% of maximum) by day 133, when green % was only just at half-maximum. Thus, although the blue % time series was more subject to confounding influences related to changes in the quality of incident solar radiation, it would appear that blue % was more sensitive to the onset of spring than was green %.

Although we evaluated a number of indices, including a normalized version of 2G\_RBi, as well as three two-channel normalized difference indices [e.g., (green % – red %)/(green % + red %)], these did not yield any new insights and, in the case of the two-channel indices, were very noisy (results not shown).

### Comparison with $f_{\text{APAR}}$ and broadband NDVI

Whereas the webcam indices 2G\_RBi (Fig. 2d), green %, and blue % (Fig. 3b, c) tended to be relatively stable during the winter phase, the same cannot be said of either the  $f_{\text{APAR}}$  or NDVI time series (Fig. 5a, b). For example, there was a clear downward trend in  $f_{\text{APAR}}$  up to day 60 (declining from 0.6 to 0.4), and then a stable period up to and including day 120. NDVI, on the other hand, was quite variable through day 80 (fluctuating between ~0.0 and ~0.3, with no clear trend), before increasing rapidly (to ~0.45) with the melting of snow. A short-lived downward spike in NDVI at day 95 was caused by fresh snow, but from day 100 up to and including day 120, NDVI remained at ~0.45. Similar to the webcam indices, both  $f_{\text{APAR}}$  and NDVI increased rapidly beginning around day 120. By day 150, the radiometric indices had more or less reached their summertime maxima (0.93 and 0.80, respectively; these values were maintained through the remaining period of the study, i.e., up to and including day 209), whereas the webcam indices (particularly green % and 2G\_RBi)

**Table 1** Best-fit parameters and model statistics for a simple logistic model,  $f(x) = a + b/(1 + e^{(c-dx)})$  of spring green-up fit to time series of canopy optical and photosynthetic properties<sup>a</sup>. The driving

variable,  $x$ , was day of year. The model was fit using mid-day data from day 100 to day 209. The value  $\psi$  is the day of year at which the function is calculated to reach its half-maximum ( $= c/d$ )

	$a$	$b$	$c$	$d$	$\psi$	$n$	$R^2$
Webcam data							
2G_RBi	-14.2	54.3	15.82	0.119	133	92	0.945
Green %	0.317	0.065	15.51	0.117	133	92	0.909
Blue %	0.282	0.045	32.95	0.263	125	92	0.468
Radiometric data							
$f_{\text{APAR}}$	0.42	0.51	30.39	0.236	129	109	0.991
NDVI	0.44	0.35	28.57	0.222	128	102	0.960
CO <sub>2</sub> flux data							
$A_{\text{max}}$	0.6	23.2	27.34	0.194	141	90	0.838

$n$  is the number of data points used to fit the model, and  $R^2$  is the regression coefficient of determination

<sup>a</sup> 2G\_RBi is an index calculated from webcam channel brightness values (DN) as  $2 \times (\text{green DN}) - (\text{red DN} + \text{blue DN})$ . Green % and blue % are normalized channel brightness values, calculated as (channel DN/total RGB DN).  $f_{\text{APAR}}$  is the fraction of incident photosynthetically active radiation absorbed by the canopy, and NDVI is a broadband normalized difference index, calculated from radiometric data.  $A_{\text{max}}$  is the light-saturated rate of canopy photosynthesis, as estimated from eddy covariance measurements of forest-atmosphere CO<sub>2</sub> exchange

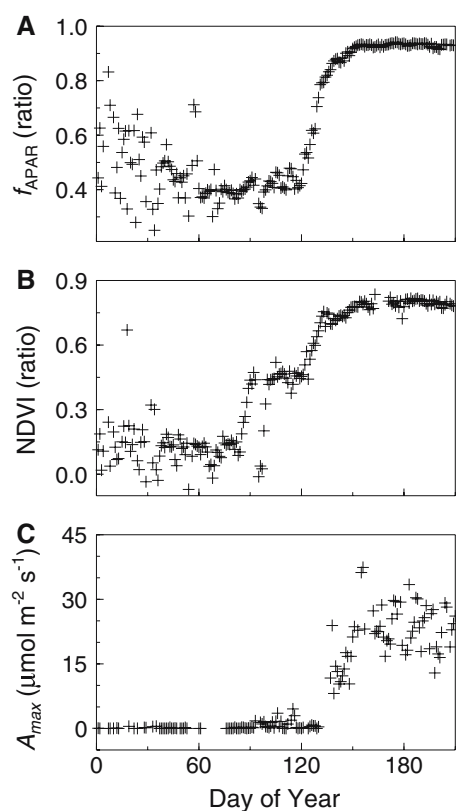


**Fig. 5** Time series of **a** the fraction of incident photosynthetically active radiation that is absorbed by the canopy ( $f_{\text{APAR}}$ ), **b** broadband normalized difference vegetation index (NDVI), calculated from measurements of surface albedo at visible (400–700 nm) and global (300–2,800 nm) wavelengths, and **c** the theoretical light-saturated rate of canopy photosynthesis ( $A_{\text{max}}$ ), estimated from eddy covariance measurements of forest-atmosphere CO<sub>2</sub> exchange. Data were recorded at the Bartlett AmeriFlux tower

continued to increase up to and including day 160 before leveling off. Overall, each of the radiometric indices exhibited noticeably less day-to-day variation around the green-up trajectory compared to any of the webcam indices, at least from about day 100 onward.

The spring green-up patterns indicated by the two radiometric indices were almost identical, as can be seen from the fact that the parameters  $c$  and  $d$  for the sigmoid phenology model were very similar for  $f_{\text{APAR}}$  and NDVI (Table 1). Indeed, the half-maximum date ( $\psi$ ) differed by only 1 day (day 129 vs. 128, respectively), between the two time series. On the other hand, the webcam indices 2G\_RBi and green % had  $\psi$  at day 133, a full 4 days later than the radiometric indices (Table 1); whereas for blue %,  $\psi$  was day 125, 3 days earlier than the radiometric indices. The fact that the value of the  $d$  parameter for the 2G\_RBi and green % model was only about half that for either the  $f_{\text{APAR}}$  or NDVI models stems from the fact that increases in these webcam indices proceeded more slowly, and were drawn out over a longer period of time, than either of the radiometric indices or blue % (Fig. 6).

Green-up patterns compared to springtime increases in  $A_{\text{max}}$

Springtime increases in  $A_{\text{max}}$  (Fig. 5c), tended to lag changes in canopy greenness, as evaluated from webcam and radiometric data (Fig. 6).  $A_{\text{max}}$  reached its half-maximum at day 141, more than a week after 2G\_RBi, and close to 2 weeks after either NDVI or  $f_{\text{APAR}}$ . In spite of this lag, the overall trajectory of increases in  $A_{\text{max}}$  more closely

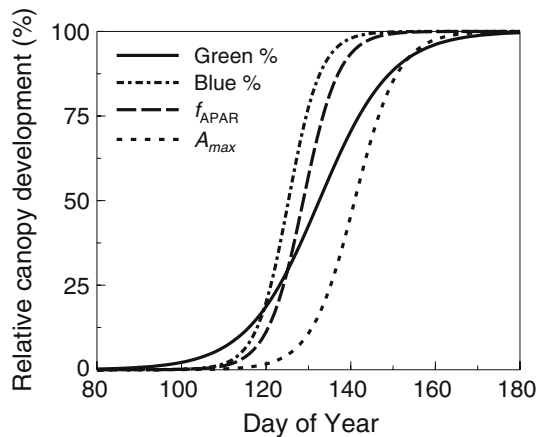


**Fig. 6** Comparison of logistic models of spring green-up, calibrated with four different characterizations of canopy state.  $f_{\text{APAR}}$  is determined using above- and below-canopy quantum sensors.  $A_{\text{max}}$  is estimated from eddy covariance measurements of forest–atmosphere  $\text{CO}_2$  exchange. Green % is the normalized brightness of the green channel, Blue % is the normalized brightness of the blue channel, from webcam images recorded from the top of the Bartlett AmeriFlux tower

paralleled those of blue %,  $f_{\text{APAR}}$ , and NDVI, rather than green % or 2G\_RBi.

## Discussion

### Evaluation of webcam and radiometric approaches

The above analysis demonstrates that a well-defined signal related to spring green-up can be extracted from images recorded using an inexpensive, commercially available webcam. The indices presented here all exhibited a clear response to changes in the canopy state resulting from spring green-up. Although some indices were highly variable from day-to-day, the sub-daily time step of the images meant that there were enough data points available to parameterize a simple sigmoid-shaped model and extract the underlying signal. However, the signal extracted depended on the particular index selected: there were differences among indices in the overall trajectory (both in terms of timing and rate of change) during the green-up phase. This is not to say that one index is “right” and all others are “wrong”, just that different indices are quantifying different canopy attributes, and the temporal variation in these canopy attributes is bound to vary somewhat. This is well-illustrated by the differences between blue and green %, with the former rising to its half-maximum not only more rapidly, but also more than a full week earlier in the growing season (this difference may be due to differences in structure and pigmentation of newly expanded and fully developed leaves; see Qi et al. 2003). The trajectory

of springtime increases in blue % was very similar to that for  $f_{\text{APAR}}$  and NDVI. Overall, the good general agreement of webcam indices with more commonly used radiometric approaches (Fig. 6) gives strong support for the validity of inferring spring green-up from analysis of webcam images.

As with other attempts to track phenology using indirect methods (either satellite remote sensing, or “near” remote sensing with optical instruments), a key shortfall with the webcam approach is that field observations are still needed if the goal is to decisively link the index measurements to particular stages of development. Leaf area index can be inferred from  $f_{\text{APAR}}$  measurements (e.g., Turner et al. 2003), or measured with a commercially available canopy analyzer (e.g., LAI 2000; Li-Cor) or hemispherical photography (e.g., HemiView; Delta-T Devices), and these ancillary data can be used to provide a context for seasonal changes in remotely sensed indices (Ahl et al. 2006). Efforts to relate continuous, remotely sensed indices and phenology-specific products (e.g., MODIS; Huete et al. 2002) to what is actually happening on the ground (e.g., Schwartz et al. 2002; Fisher et al. 2006; Ahl et al. 2006) are clearly essential, especially given current interest in scaling from intensively monitored sites to more extensive spatial domains, such as across ecosystem types to entire regions (e.g., North American Carbon Program; Wofsy and Harriss 2002).

An alternative use of these data is as a measure of physiological activity or capacity, e.g., as a scalar for either photosynthetic potential or light use efficiency (LUE) in  $\text{CO}_2$ -exchange modeling. For example, Drolet et al. (2005) recently established strong correlations between a version of the photochemical reflectance index (PRI; see Gamon et al. 1997), calculated using MODIS ocean band 11, and flux tower-derived estimates of LUE, but the authors cautioned that confounding factors (other than xanthophyll cycle pigments, which is what PRI was originally designed to detect) may have been responsible for the observed patterns. To date the physiological implications of dynamic changes in vegetation reflectance (especially as sensed by satellites) are poorly understood (Hill et al. 2006). Although Jenkins et al. (2007) used year 2004 data from the Bartlett tower to examine seasonal changes in gross canopy photosynthesis,  $f_{\text{APAR}}$ , and broadband NDVI, the scaling between photosynthesis and either  $f_{\text{APAR}}$  or NDVI during green-up was not explicitly quantified. Based on the present study, it seems that in this deciduous forest, regardless of the optical approach used (webcam or radiometry) to infer spring green-up, changes in  $A_{\text{max}}$  lag changes in green-up by at least a week, and possibly 2 weeks (Fig. 6). This is largely to be expected, since leaf level studies indicate that area-based photosynthetic rates may continue to increase even after leaf expansion has ceased (e.g., Bassow and Bazzaz 1998; Morecroft et al. 2003); this is

likely due to continued increases in leaf mass to area ratio, which is correlated with photosynthetic capacity (Wright et al. 2004). Similarly, maximum canopy-level carboxylation rate in a mixed temperate deciduous forest has been shown to continue to increase even after peak LAI has been achieved (Wilson et al. 2001). Thus, as noted by Sakai et al. (1997), the canopy is physiologically active for a shorter period of time than would tend to be indicated by the mere presence of leaves.

#### Evaluation of advantages and disadvantages of webcams

We acknowledge that an obvious disadvantage of the webcam approach is the pronounced variability in normalized channel brightness (channel %) resulting from changes in quality and quantity of incident solar radiation (Fig. 4). A reference panel placed in one corner of the camera image could be used to standardize images taken under different lighting or weather conditions. This internal standard would be somewhat comparable to the way in which a spectralon panel is used to determine the spectral characteristics of the illuminating lamp, and normalize reflectance measurements made with a portable spectrometer (e.g., Richardson et al. 2001). Further analyses of time periods containing particular types of environmental conditions, or time periods when outliers tend to occur, could provide further insight into the sources of variability in the data.

However, tracking phenology with a webcam also has a number of advantages over either traditional (based on direct field observation) or radiometric (e.g.,  $f_{\text{APAR}}$  and NDVI) approaches. Compared to automated, camera- or instrument-based approaches, field observations of phenology are labor intensive and expensive, since surveys must be conducted at a sufficiently high temporal frequency so that key dates (e.g., budburst) can be identified with some precision. Furthermore, an adequate number of individual trees must be inspected to ensure adequate sampling of a population. There is the potential for observer bias: results presented by Schaber (2002) indicate that variation among observers in identifying the date of budburst is  $\sim \pm 3$  days (at 95% confidence), which is less than the genetic variability in budburst dates measured among individuals of the same species.

By comparison, webcam and radiometric measurements provide a continuous record (storage of data at a half-hourly time step is feasible) with little effort required once the initial installation is complete—excluding, of course, periodic inspection and inevitable maintenance and calibration. It is straightforward to implement a standardized measurement protocol across sites: to minimize bias, it would of course be preferable that the same instruments or

camera, in the same configuration, be used. There need not be any subjectivity involved in processing of webcam images, which can be conducted entirely by an automated script: as noted in the [Materials and methods](#), we used every available webcam image, rather than attempt to filter out of images that did not meet arbitrary quality control criteria.

Webcam images have the added bonus of providing a permanent record that can be inspected at any time. In addition to providing a more intuitive sense of the state of the canopy (compared to a single  $f_{\text{APAR}}$  or NDVI value, for example), these images could also prove extremely useful for diagnosing apparent inconsistencies in other data streams. For example, by looking at our archived images, it was possible to identify the late snowfall on day 95 that caused what would otherwise appear to be aberrant NDVI readings.

Webcam images provide greater spatial integration (and sampling of multiple species) than the effective point-scale of radiometric instruments (Oliphant et al. 2006). For example, we estimate that there are in the order of 50 trees included in the webcam ROI, whereas two or three trees dominate the field of view of the broadband NDVI instruments. This degree of integration is highly desirable in the context of  $\text{CO}_2$  flux measurements, since the footprint of the measurement system extends for several hundred meters, and is not centered on the tower.

Compared to radiometric instruments, a webcam is relatively inexpensive. The model we used here cost roughly \$1,175 (camera, \$850; weatherproof housing, \$250; software, \$75; much less expensive cameras are available, as are more expensive cameras offering remote pan, tilt and zoom functions), not including the PC required for image capture and archiving. The eight quantum sensors we use to measure  $f_{\text{APAR}}$  cost a total of roughly \$4,000, and the two quantum sensors and two pyranometers (\$825 each) used to measure broadband NDVI cost a total of roughly \$2,650. Note that the costs reported for radiometric instruments assume that a datalogger with a sufficient supply of free channels is already available. The lower cost means that for roughly the same amount of money, an array of two or three webcams could be used for more extensive sampling than is possible with a single  $f_{\text{APAR}}$  or broadband NDVI setup.

Phenology studies have a long history in Europe and Japan, but data are comparatively lacking in North America; in that regard, the recently-formed USA National Phenology Network (NPN) has been established to coordinate the collection and dissemination of phenological data (Betancourt et al. 2005). Given the widespread popularity of webcams, and the fact that they are already ubiquitous in our landscape (commonly mounted on campus buildings, at national parks, in town squares, etc.), our

results suggest that images from such cameras could offer a novel opportunity to provide data that would complement the efforts of the NPN, at relatively low cost. This could easily be integrated into hands-on science education programs for primary and secondary school students (e.g., the international GLOBE endeavor, <http://www.globe.gov/>), which would provide chances for public outreach by the earth systems science community.

**Acknowledgements** Bob Evans and Chris Costello are thanked for their assistance with tower operations. Support for this research was provided by the NASA Terrestrial Carbon Program (grant no. CARBON/04–0120–0011) and by the NASA IDS program (grant no. NNG04GH75G). Research at the Bartlett Experimental Forest is supported by the USDA Forest Service’s Northern Global Change program, and tower measurements are partially funded by the USDA Forest Service’s Northern Research Station. Meteorological and radiometric data, as well as CO<sub>2</sub> and H<sub>2</sub>O fluxes, for the Bartlett tower are available at <http://www.public.ornl.gov/ameriflux/> subject to AmeriFlux Fair-use policies.

## References

- Ahl DE, Gower ST, Burrows SN, Shabanov NV, Myneni RB, Knyazikhin Y (2006) Monitoring spring canopy phenology of a deciduous broadleaf forest using MODIS. *Remote Sens Environ* 104:88–95
- Badeck F-W, et al. (2004) Responses of spring phenology to climate change. *New Phytol* 162:295–309
- Baldocchi D, et al. (2001) FLUXNET: a new tool to study the temporal and spatial variability of ecosystem-scale carbon dioxide, water vapor, and energy flux densities. *Bull Am Meteorol Soc* 82:2415–2434
- Baldocchi DD, et al. (2005) Predicting the onset of carbon uptake by deciduous forests with soil temperature and climate data: a synthesis of FLUXNET data. *Intl J Biometeorol* 49:377–387
- Bassow SL, Bazzaz FA (1998) How environmental conditions affect canopy leaf-level photosynthesis in four deciduous tree species. *Ecology* 79:2660–2675
- Betancourt JL, et al. (2005) Implementing a U.S. National phenology network. *EOS Trans* 86:539–541
- Chuine I, Yiou P, Viovy N, Seguin B, Daux V, Le Roy Ladurie E (2004) Grape ripening as a past climate indicator. *Nature* 432:289–290
- Churkina G, Schimel D, Braswell BH, Xiao XM (2005) Spatial analysis of growing season length control over net ecosystem exchange. *Global Change Biol* 11:1777–1787
- Drolet GG, et al. (2005) A MODIS-derived photochemical reflectance index to detect inter-annual variations in the photosynthetic light-use efficiency of a boreal deciduous forest. *Remote Sens Environ* 98:212–224
- Fisher JI, Mustard JF, Vadeboncoeur MA (2006) Green leaf phenology at Landsat resolution: scaling from the field to the satellite. *Remote Sens Environ* 100:265–279
- Fitter AH, Fitter RSR (2002) Rapid changes in flower time in British plants. *Science* 296:1689–1691
- Gamon JA, Serrano L, Surfus JS (1997) The photochemical reflectance index: an optical indicator of photosynthetic radiation use efficiency across species, functional types, and nutrient levels. *Oecologia* 112:492–501
- Gates DM (1966) Spectral distribution of solar radiation at the Earth’s surface. *Science* 151:523–529
- Goulden ML, Munger JW, Fan SM, Daube BC, Wofsy SC (1996) Measurements of carbon sequestration by long-term eddy covariance: methods and a critical evaluation of accuracy. *Global Change Biol* 2:169–182
- Hill MJ, Held AA, Leuning R, Coops NC, Hughes D, Cleugh HA (2006) MODIS spectral signals at a flux tower site: Relationships with high-resolution data, and CO<sub>2</sub> flux and light use efficiency measurements. *Remote Sens Environ* 103:351–368
- Hollinger DY, Richardson AD (2005) Uncertainty in eddy covariance measurements and its application to physiological models. *Tree Physiol* 25:873–885
- Hollinger DY, Goltz SM, Davidson EA, Lee JT, Tu K, Valentine HT (1999) Seasonal patterns and environmental control of carbon dioxide and water vapour exchange in an ecotonal boreal forest. *Global Change Biol* 5:891–902
- Hollinger DY, et al. (2004) Spatial and temporal variability in forest-atmosphere CO<sub>2</sub> exchange. *Global Change Biol* 10:1689–1706
- Huemmrich KF, Black TA, Jarvis PG, McCaughey JH, Hall FG (1999) High temporal resolution NDVI phenology from micro-meteorological radiation sensors. *J Geophys Res Atmos* 104:27935–27944
- Huete A, Didan K, Miura T, Rodriguez EP, Gao X, Ferreira LG (2002) Overview of the radiometric and biophysical performance of the MODIS vegetation indices. *Remote Sens Environ* 83:195–213
- Jenkins JP, Braswell BH, Froelking SE, Aber JD (2002) Detecting and predicting spatial and interannual patterns of temperate forest springtime phenology in the eastern U.S. *Geophys Res Lett* 29:2201, doi:10.1029/2001GL014008
- Jenkins JP, Richardson AD, Braswell BH, Ollinger SV, Hollinger DY, Smith ML (2007) Refining light-use efficiency calculations for a deciduous forest canopy using simultaneous tower-based carbon flux and radiometric measurements. *Agric For Meteorol* 143:64–79
- Lieth H (1975) Modeling primary productivity of the world. In: Lieth H, Whittaker RH (eds) *Primary productivity of the biosphere*, vol 14. Springer, New York, pp 237–263
- Lucht W, et al. (2002) Climatic control of the high-latitude vegetation greening trend and Pinatubo effect. *Science* 296:1687–1689
- Moore KE, Fitzjarrald DR, Sakai RK, Goulden ML, Munger JW, Wofsy SC (1996) Seasonal variation in radiative and turbulent exchange at a deciduous forest in central Massachusetts. *J Appl Meteorol* 35:122–134
- Morecroft MD, Stokes VJ, Morison JIL (2003) Seasonal changes in the photosynthetic capacity of canopy oak (*Quercus robur*) leaves: the impact of slow development on annual carbon uptake. *Int J Biometeorol* 47:221–226
- Nemani RR, et al. (2003) Climate-driven increases in global terrestrial net primary production from 1982 to 1999. *Science* 300:1560–1563
- Oliphant A, Grimmond SCB, Schmid HP, Wayson CA (2006) Local-scale heterogeneity of photosynthetically active radiation (PAR), absorbed PAR and net radiation as a function of topography, sky conditions and leaf area index. *Remote Sens Environ* 103:324–337
- Peñuelas J, Filella I, Comas P (2002) Changed plant and animal life cycles from 1952 to 2000 in the Mediterranean region. *Global Change Biol* 8:531–544
- Qi J, Moran MS, Cabot F, Dedieu G (1995) Normalization of sun/view angle effects using spectral albedo-based vegetation indices. *Remote Sens Environ* 52:207–217
- Qi Y, Bai S, Heisler GM (2003) Changes in ultraviolet-B and visible optical properties and absorbing pigment concentrations in pecan leaves. *Agric For Meteorol* 120:229–240
- Richardson AD, Berlyn GP, Gregoire TG (2001) Spectral reflectance of *Picea rubens* (Pinaceae) and *Abies balsamea* (Pinaceae)

- needles along an elevational gradient, Mt. Moosilauke, New Hampshire, USA. *Am J Bot* 88:667–676
- Richardson AD, Bailey AS, Denny EG, Martin CW, O'Keefe J (2006a) Phenology of a northern hardwood forest canopy. *Global Change Biol* 12:1174–1188
- Richardson AD, et al. (2006b) A multi-site analysis of random error in tower-based measurements of carbon and energy fluxes. *Agric For Meteorol* 136:1–18
- Running SW, Nemani RR (1991) Regional hydrologic and carbon balance responses of forests resulting from potential climate change. *Clim Change* 19:349–368
- Sakai RK, Fitzjarrald DR, Moore KE (1997) Detecting leaf area and surface resistance during transition seasons. *Agric For Meteorol* 84:273–284
- Schaber J (2002) Phenology in Germany in the 20th century: methods, analyses and models. In: Department of Geoecology. University of Potsdam, Potsdam, p 146
- Schwartz MD, Reed BC, White MA (2002) Assessing satellite-derived start-of-season measures in the coterminous USA. *Int J Climatol* 22:1793–1805
- Sit V, Poulin-Costello M (1994) Catalog of curve fitting (biometrics information handbook series, no. 4). British Columbia Ministry of Forests, Victoria
- Sparks TH, Menzel A (2002) Observed changes in seasons: an overview. *Int J Climatol* 22:1715–1725
- Suni T, et al. (2003) Air temperature triggers the recovery of evergreen boreal forest photosynthesis in spring. *Global Change Biol* 9:1410–1426
- Turner DP, et al. (2003) A cross-biome comparison of daily light use efficiency for gross primary production. *Global Change Biol* 9:383–395
- Wang Q, Tenhunen J, Dinh NQ, Reichstein M, Vesala T, Keronen P (2004) Similarities in ground- and satellite-based NDVI time series and their relationship to physiological activity of a Scots pine forest in Finland. *Remote Sens Environ* 93:225–237
- White MA, Thornton PE, Running SW (1997) A continental phenology model for monitoring vegetation responses to inter-annual climatic variability. *Global Biogeochem Cycles* 11:217–234
- White MA, Running SW, Thornton PE (1999) The impact of growing-season length variability on carbon assimilation and evapotranspiration over 88 years in the eastern US deciduous forest. *Int J Biometeorol* 42:139–145
- Wilson KB, Baldocchi DD, Hanson PJ (2001) Leaf age affects the seasonal pattern of photosynthetic capacity and net ecosystem exchange of carbon in a deciduous forest. *Plant Cell Environ* 24:571–583
- Wofsy SC, Harriss RC (2002) The North American carbon program (NACP): a report of the NACP Committee of the U.S. carbon cycle science steering group. In: U.S. Global Change Research Program, Washington
- Wright IJ, et al. (2004) The worldwide leaf economics spectrum. *Nature* 428:821–827
- Wythers KR, Reich PB, Turner DP (2003) Predicting leaf area index from scaling principles: corroboration and consequences. *Tree Physiol* 23:1171–1179